Welding in the World (2026) 70:2835–2845
https://doi.org/10.1007/s40194-025-02209-w

RESEARCH PAPER

# Copper/stainless steel cladding by explosive welding: effect of the energetic mixture

**Ivan Galvão[1,3] · Gustavo H. S. F. L. Carvalho[2,3] · Rui M. Leal[3,4] · Ricardo Mendes[5]**

Received: 29 July 2025 / Accepted: 10 October 2025 / Published online: 7 November 2025


**Abstract**
Copper/stainless steel clads are very appealing for numerous industries by combining their specific properties into a single component. This study investigates the production of these clads by explosive welding, emphasising the influence of varying energetic substances and parameters on the interfacial morphology, mechanical properties, and overall quality of the welded joints. Two weld series were produced using different energetic mixtures, one with a higher density and a detonation velocity of 2420 m.s$^{-1}$ and the other with a lower density and a detonation velocity of 3320 m.s$^{-1}$. Successful clads were achieved, allowing the production of components with a very good mechanical behaviour without the use of expensive interlayer plates. The clads produced with the higher detonation velocity mixture, which provided a lower explosive ratio and a lower impact velocity, presented a smoother surface finish with fewer irregularities. In terms of weld interface morphology, interfaces composed of well-defined waves with a typical morphology were achieved for both series. The wavelength and amplitude were found to vary according to the used energetic mixture, as they depend on the impact velocity, the explosive ratio, and the energy lost in the collision. The tensile-shear tests yielded excellent results, with welded joints demonstrating superior strength compared to the parent materials, as evidenced by fracturing occurring outside the weld region. The interfacial hardening of the welds was influenced by the energetic mixture, contributing to an improvement in the clad maximum tensile-shear load.

**Keywords** Stainless steel · Copper · Cladding · Explosive welding · Energetic mixture · Interface

## 1 Introduction

In recent years, there has been a growing need to join materials with distinct characteristics to obtain a unique hybrid final component with properties that could not be achieved with a single material. Stainless steel, known for its excellent corrosion resistance and durability, is an essential material across many industries, including construction, medical, the food industry, and oil and gas. Copper alloys, on the other hand, are known for their excellent electrical and thermal conductivities and good corrosion resistance, making them essential in electronics and heat exchangers.

The importance of welding stainless steel to copper alloys arises from the need to combine their distinct properties in a single component. For instance, in electrical applications, a connection might require the high conductivity of copper at the contact point and the structural strength and corrosion resistance of stainless steel for the housing. The combination is also applied in nuclear fusion equipment as coil terminals [1]. Welding these dissimilar

Recommended for publication by Commission III - Resistance Welding, Solid State Welding, and Allied Joining Process.

✉ Gustavo H. S. F. L. Carvalho
gustavo.carvalho@unifi.it

1 UnIRE, Department of Mechanical Engineering, ISEL - Polytechnic University of Lisbon, Lisbon, Portugal

2 Department of Industrial Engineering, University of Florence, Florence, Italy

3 Univ Coimbra, CEMMPRE, Department of Mechanical Engineering, Coimbra, Portugal

4 LIDA-ESAD.CR, Polytechnic University of Leiria, Caldas da Rainha, Portugal

5 Univ Coimbra, ADAI, LEDAP, Department of Mechanical Engineering, Rua Luís Reis Santos, Pólo II, 3030-788 Coimbra, Portugal

metals with conventional techniques is significantly challenging due to their differences in melting temperature, thermal conductivity, and thermal expansion.

Several welding techniques are used for joining stainless steel and copper alloys. Fusion welding processes, such as gas tungsten arc welding (GTAW) and gas metal arc welding (GMAW), can be used but require precise process control to prevent cracking, porosity, residual stresses, and distortion caused by their differences in physical properties. Solid-state welding techniques, such as explosive welding (EXW), offer an alternative approach that minimises heat input and reduces the risk of cracking and other defects related to solidification. However, there are still challenges in the explosive welding of stainless steel to copper regarding interfacial phenomena and the selection and optimisation of energetic parameters.

EXW is a solid-state welding process characterised by the joining of metallic materials through a high-velocity collision caused by a controlled detonation of an explosive [2]. Interest in this process has increased significantly because of its low cost, rapid fabrication, and the ability to weld nearly all available metal materials, even those with very different properties.

Explosive welding of stainless steel to copper has been a research subject for the past 10 to 20 years. Durgutlu et al. [3, 4] have conducted extensive research on this material combination, focusing on the geometrical effects of the process (stand-off distance) and the energetic material ratio. Bina et al. [5] investigated heat treatments for this combination, a crucial topic for understanding the interaction of the components at high temperatures. More recently, Wang et al. [1] studied the combination for use in nuclear fusion equipment, addressing important issues such as the weldability window and mechanical properties. Also analysing the weldability window and the weld interface, Liu et al. [6] studied the combination, performing an integrated analysis of the interface and weldability window. In-depth microstructural studies of the metallic pair have also been conducted to further understand the complex phenomena occurring at the interface and their effect on properties [7, 8].

More recently, Carvalho et al. [9] conducted an analysis of the physical properties of copper/stainless steel welds, highlighting the effect of each physical property on the quality of the welded joint and the morphology of the interface. Numerical simulations have also gained attention to simulate thick stainless steel to copper joining [10].

However, there are still some challenges that need to be overcome in terms of parameter optimisation, cladding quality, and a more integrative analysis of this material combination. The ability to weld stainless steel and copper alloys is crucial for various fields. From creating more efficient heat exchangers to developing robust electrical connections, this capability allows the design and fabrication of complex components with enhanced performance.

This study investigates the joining of stainless steel and copper, with a particular emphasis on the influence of varying energetic parameters on the interfacial morphology, mechanical properties, and overall quality of the welded joint. A comprehensive microstructural analysis was undertaken, employing optical microscopy, 3D digital microscopy, and scanning electron microscopy (SEM) coupled with energy-dispersive X-ray spectroscopy (EDS) to determine elemental distribution. Furthermore, electron backscatter diffraction (EBSD) was utilised to provide a detailed characterisation of the interfacial regions. Mechanical testing, including microhardness and tensile-shear testing, supplemented by digital image correlation (DIC), was performed to evaluate the mechanical performance of the welded joints.

## 2 Experimental procedure

Two series of EXW joints were performed to join 3-mm-thick plates of C12200 copper (Cu) and AISI 304/AISI 316 austenitic stainless steels (SS). The welds were produced in a full overlap parallel configuration, using the Cu plate as the flyer and the SS as the baseplate. As displayed in Table 1, two weld series were produced using distinct explosive mixtures, i.e. a lower detonation velocity (LD series) and a higher detonation velocity (HD series) energetic material. The LD series used an ANFO-based mixture, and the HD series used an ammonium nitrate-based emulsion (AN-E), which was sensitised with expanded polystyrene spheres (EPS) to regulate the detonation velocity [11, 12]. The explosive ratios (R), which correspond to the ratio of the mass of the explosive mixture to the mass of the flyer plate, were 1.00 in the LD weld series and 0.44 in the HD series. The stand-off distance (STD) was the same in all welds (4.5 mm).

The procedure adopted to measure the detonation velocity of the explosive mixtures followed that conducted by

**Table 1** Welding conditions for the LD and HD weld series

| Welding conditions | LD | HD |
|---|---|---|
| Flyer plate | C12200 | |
| Base plate | AISI 304, AISI 316 | |
| Configuration | Full overlap | Full overlap |
| Explosive mixture | ANFO | AN-E+EPS |
| Explosive mixture density | 864 kg.m$^{-3}$ | 584 kg.m$^{-3}$ |
| Flyer plate thickness | 3 mm | 3 mm |
| Base plate thickness | 3 mm | 3 mm |
| R | 1.00 | 0.44 |
| STD | 4.5 mm | 4.5 mm |

Mendes et al. [13] and Quaresma et al. [14]. The weld surfaces (flyer plate side) were analysed using a Hirox HRX-01 3D digital microscope. Samples of the longitudinal cross-section of the welds were collected and prepared for metallographic analysis according to ASTM E3-11. The microstructural characterisation of the welds was conducted by optical microscopy, using a Leica DM4000M LED microscope, and by SEM, using a Hitachi SU3800 microscope equipped with EDS. Complementary microstructural analysis was performed by EBSD, using an FEI Quanta 400FEG ESEM microscope. The EBSD maps were achieved using TSL OIM Analysis software application.

The mechanical properties of the welds were characterised by microhardness and tensile-shear testing. Microhardness testing was conducted in a Struers Duramin equipment, using testing loads of 200 gf and a testing time of 15 s. Three hardness profiles were registered along the thickness of the longitudinal cross-section of each weld, with a distance between consecutive indentations of 500 µm. Localised hardness measurements were performed with a lower testing load of 50 gf over the weld interface. Three tensile-shear specimens per weld, with a similar design to that reported by Carvalho et al. [15, 16] were tested. This design allows the weld interface to be subjected to shear effort during tensile testing, being an effective procedure to characterise the interface of full overlap joints. However, the shear strength obtained using this test does not correspond to a unique material property and cannot be used as a design parameter [17]. The tests were performed with a testing speed of 1 mm/min, using a 100 kN universal testing machine Shimadzu AGS-X. The strain fields of the specimens were obtained by DIC using a GOM Aramis 5 M system, following the specimen preparation methodology developed by Leitão et al. [18] for processing and analysing the strain data.

## 3 Results and discussion

### 3.1 Welding parameters

Table 2 displays the measured detonation velocity ($V_d$) (which is the same as the collision point velocity, $V_c$, for a parallel configuration), the calculated impact velocity ($V_p$), and the welding results. The impact velocity was calculated with Gurney's equation for a one-dimensional problem in parallel configuration (Eq. 1) [19, 20]. This computation procedure, although it presents well-known limitations by ignoring the acceleration of the flyer plate along the STD and representing only the terminal velocity, is widely accepted in the literature [20, 21]. The table also shows the values of the energy lost in collision for both welds (ΔKE), which correspond to the kinetic energy per unit area of the flyer plate at the impact.

**Table 2** Detonation/collision point and impact velocities, energy lost in collision, and welding results

| Weld series | $V_d$, $V_c$ ($m.s^{-1}$) | $V_p$ ($m.s^{-1}$) | ΔKE ($MJ.m^{-2}$) | Welding results |
|---|---|---|---|---|
| LD | 2420 | 446 | 2.76 | Sound |
| HD | 3320 | 334 | 1.54 | Sound |

$$V_{pF} = \sqrt{2E}\left(\frac{3R^2}{R^2+5R+4}\right)^{\frac{1}{2}} \quad (1)$$

$\sqrt{2E}$ is the Gurney characteristic velocity ($m.s^{-1}$) of the explosive mixture. This parameter was estimated according to Cooper's [22] approach for ideal explosives.

It can be observed that the HD mixture provided a $V_c$ about 40% greater than the $V_c$ of the LD mixture. Despite this difference in $V_c$, the HD mixture presented lower $V_p$ and ΔKE (about 75%) due to the lower explosive ratio used to produce the welds. This mixture, besides having a lower density than the LD mixture, requires a lower explosive thickness to detonate and maintain an adequate $V_c$. This fact results in a smaller amount of energetic material, leading to a lower ratio, lower $V_p$, and consequently a lower ΔKE. Regardless of the explosive mixtures used, sound welding results were achieved, with no visible macro defects being detected in the joints. Regarding the impact of the mixture on the surface, the two energetic mixtures presented different results. Figure 1a and b shows the analysis of the weld surfaces on the copper side (flyer plate surface in contact with the energetic mixture). A smoother surface finish with fewer surface irregularities was achieved with the HD mixture (AN-E+EPS). This mixture provided less plastic strain at the surface of the Cu flyer plate, resulting in a better surface quality for these joints, which agrees with what was observed by Mendes et al. [23]. The stainless steel surface, which was not in contact with the energetic material, did not present significant differences among both weld series.

According to Zakharenko [24] and Efremov and Zakharenko [25], sound welding conditions are achieved when the solidification of the localised molten material occurs before tensile-stress waves arise at the weld interface. Otherwise, if the tensile-stress waves reach the weld interface before the solidification of the molten zones, the materials will separate, and no consistent bond will be achieved. The required time for the solidification of the molten material ($t_s$) and the time for the arising positive pressures at the weld interface after the impact ($t_p$) can be computed using Eqs. 2 and 3.

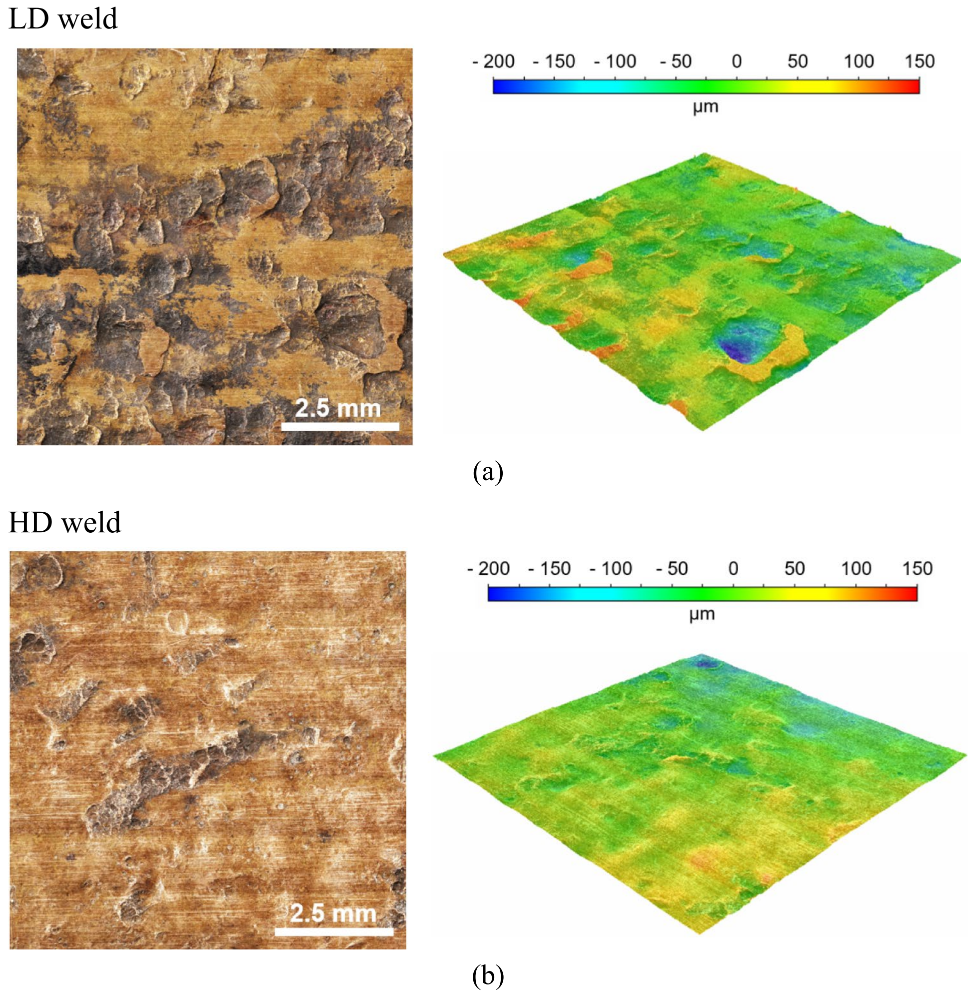


**Fig. 1** Morphology of the external weld joint surfaces on the copper side: **a** LD weld, **b** HD weld

$$t_p = \left[0.5 + 0.66\left(\frac{\rho_{flyer} \bullet V_c^{\ 2}}{G_{flyer}}\right)\right] \bullet \frac{\delta_{flyer}}{V_c} \quad (2)$$

$\rho_{flyer}$, $\delta_{flyer}$, and $G_{flyer}$ are the density (kg.m$^{-3}$), thickness (m), and shear modulus (Pa) of the flyer plate, respectively.

$$t_s = \frac{Q^2}{4 \bullet \pi \cdot c_{flyer} \cdot \lambda_{flyer} \bullet \rho_{flyer} \cdot T_{mflyer}^{\ 2}},$$
$$Q = 6.8 \bullet 10^{-2} \bullet V_c^2 \bullet \rho_{flyer} \bullet \delta_{flyer} \bullet \frac{\delta_{base}}{\delta_{flyer} + \delta_{base}} \bullet \sin^2\left(\frac{\beta}{2}\right) \quad (3)$$

$Q$ is the heat released at the weld interface (J.m$^{-2}$). $c_{flyer}$, $\lambda_{flyer}$, and $T_{mflyer}$ are the specific heat (J.kg$^{-1}$.C$^{o-1}$), thermal conductivity (W.m$^{-1}$.C$^{o-1}$), and melting temperature (C$^o$) of the flyer plate. $\delta_{base}$ is the thickness of the baseplate (m), and $\beta$ is the impact angle (rad).

Figure 2a and b presents the equations plotted for each weld series. It can be observed that sound welding conditions are expected for both series based on this theory. In fact, the tested collision point velocities used are well below the critical collision point velocity ($V_c^{crt}$) at the intersection of the $t_p$ and $t_s$ curves, which represents the theoretical maximum velocity for effective bonding.

### 3.2 Weld interface morphology

Figure 3a and b presents the micrographs of the longitudinal cross-section of the welds. The micrographs show that both weld series present interfaces composed of well-defined waves with a typical morphology, i.e. without the curled pattern observed for many material couples like Al-Cu [26], Al-CS [27] or Al-Mg [28]. The interfacial morphology in EXW is a crucial aspect of the cladding because it provides valuable insights into the quality of the bond, material mixing, and how potential brittle phases can be distributed at the interface. There are some theories developed to predict the interface morphology, such as the wave interface factor (WIF) [29] and the impedance mismatch parameter (IMP) [16]. According to these authors, the WIF, which considers

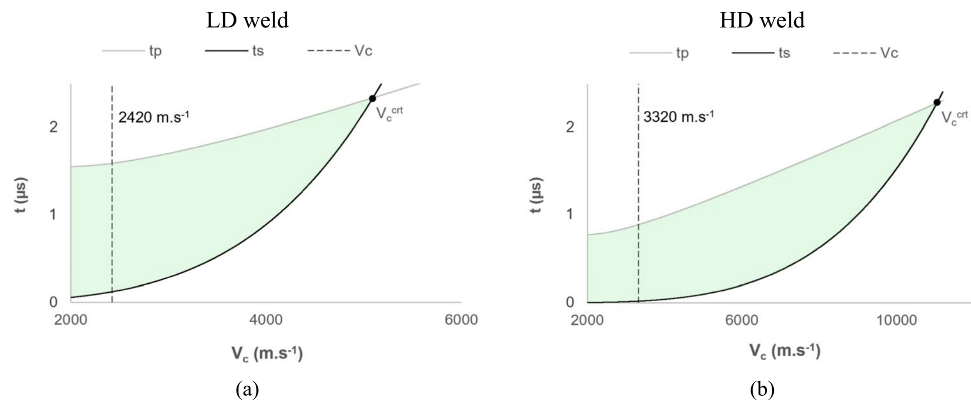


**Fig. 2** Time-velocity diagrams: **a** LD weld series, **b** HD weld series

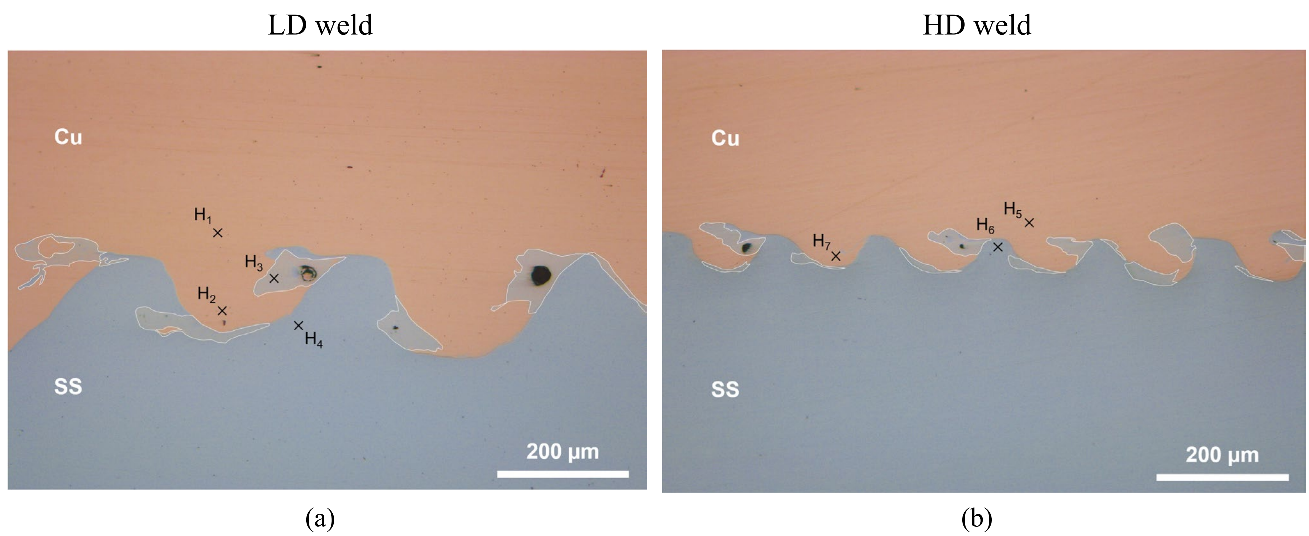


**Fig. 3** Morphology of the weld interface: **a** HD series, **b** LD series and the microhardness localised measurements presented in Table 5

the differences in density and melting temperature of the welded materials and their relative position in the joint (flyer or baseplate), can be used to predict the possibility of the formation of a wavy interface for a specific couple of materials (Eq. 4). For Cu-SS welding, the WIF value points to the formation of a wavy interface (Table 3), which was effectively observed for these welds. In the same way, the typical shape of the waves meets the IMP theory developed by Carvalho et al. [16], which correlates the wave shape to the ratio of the flyer to the baseplate impedances (Eq. 5). A low IMP value points to the formation of waves with a similar pattern to those observed at the interface of the HD and LD welds (Table 3).

$$\mathrm{WIF} = \frac{\rho_{\mathrm{flyer}}}{\rho_{\mathrm{base}}} \bullet \frac{\mathrm{T}_{\mathrm{m\,flyer}}}{\mathrm{T}_{\mathrm{m\,base}}} \tag{4}$$

$$\mathrm{IMP} = \left|1 - \mathrm{Z}_{\mathrm{ratio}}\right| = \left|1 - \frac{\mathrm{Z}_{\mathrm{flyer}}}{\mathrm{Z}_{\mathrm{base}}}\right| = \frac{\rho_{\mathrm{flyer}}.\mathrm{C}_{\mathrm{b\,flyer}}}{\rho_{\mathrm{base}}.\mathrm{C}_{\mathrm{b\,base}}} \tag{5}$$

$Z$ is the impedance (kg.m$^{-2}$.s$^{-1}$) and $C_b$ is the bulk sound velocity propagation in the material (m.s$^{-1}$).

Despite the similar morphological pattern/shape of the interfaces of both weld series, important differences were observed in the wave geometrical parameters, i.e. amplitude and wavelength (Table 3). The interface of the HD weld series, which was produced with a higher $V_d$ and lower $V_p$, is composed of waves with approximately 40% lower amplitude and wavelength. The lower $V_p$ of the HD welds resulted in a much lower energy release during the impact, leading to the formation of less pronounced interfacial waves. The $V_p$ parameter depends on the explosive mixture and is directly related to the explosive ratio. Hence, the final geometrical parameters of the interface are directly affected by the explosive ratio. Since the general morphology is similar (wavy),

**Table 3** Wave parameters of the welds

| Weld series | WIF | IMP | Amplitude (μm) | Wavelength (μm) |
|---|---|---|---|---|
| LD | 0.87 (wavy[a]) | 0.052 (typical[a]) | 157 | 430 |
| HD | | | 64 | 171 |

[a]Expected morphology based on the computed parameter

the morphological pattern/shape of the interfacial waves is mainly affected by the difference in the physical properties of the welded materials and their relative position in the joint. In contrast, the wave geometrical parameters mostly depend on the impact parameters ($V_p$, explosive ratio, and ΔKE).

Formation of material pockets can be observed aside from each wave crest and trough for both weld series (light grey zones in Fig. 3). These regions are often reported in the literature and correspond to vortex zones, in which maximum temperature and plastic strain values are reached [30]. In good agreement with this, micro-cavities were formed in some of these zones, which points to localised melting during welding. Depending on the combination of materials being welded, the material pockets may present very different morphologies, with higher or lower homogeneity and with or without intermetallic composition [31, 32]. It should be noted, however, that the phase diagram of Fe-Cu and Cu-Cr, the main elements, does not indicate the formation of intermetallic phases. That said, the mixed regions between copper flyer and stainless steel base are not expected to contain brittle intermetallic compounds.

Comparing the SEM analysis in Fig. 4a and b, it is possible to deduce that the size of these zones was influenced by the impact parameters ($V_p$, explosive ratio, and ΔKE), as observed in the geometrical parameters of the interfacial waves. Larger regions are observed in the welds produced with the LD mixture, which meets the higher energy conditions associated with the impact velocity in this series. On

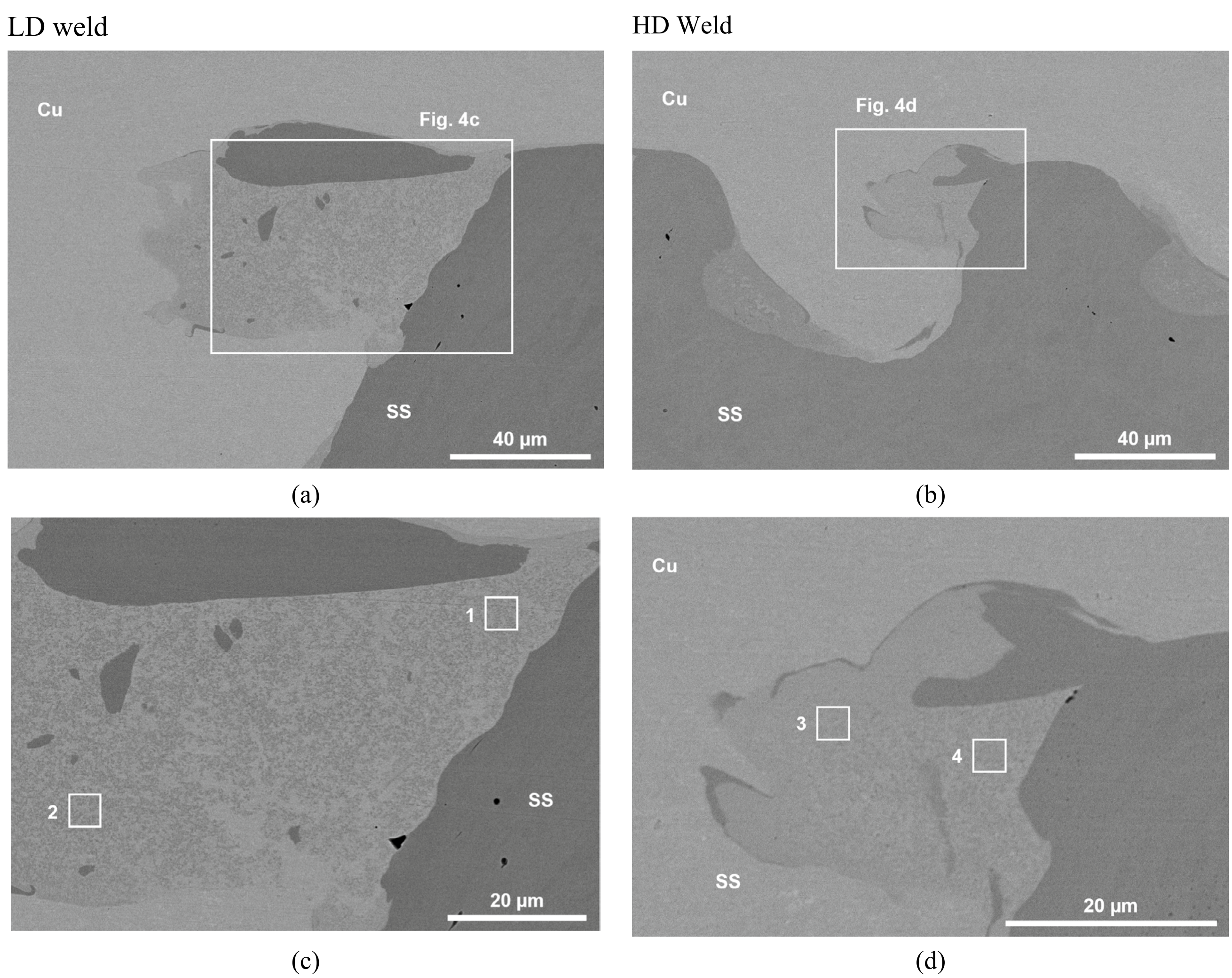


**Fig. 4** Morphology of the vortex zones: **a**, **c** LD series, **b**, **d** HD series

the other hand, the morphological properties of the material pockets were not influenced by the impact parameters or even the type of the explosive mixture since zones with similar morphology were observed for both weld series. Figure 4c and d shows that these zones are composed of a light-colour matrix with some darker particles of irregular size dispersed over it. According to Table 4, which shows the results of the EDS analysis conducted in the areas indicated in the micrographs, the matrix is composed of Cu, Fe, and the remaining alloy elements of the SS. Cu is the major chemical element in the pockets, whose chemical composition (at.%) is more than three times greater than that of Fe. These results meet the findings from Galvão et al.[33], who concluded that the interaction regions associated with the vortex zones in EXW or bimetallic clads are richer in the material with a lower melting temperature.

Figure 5a and b shows the EDS elemental mapping of the vortex zones for both weld series. The irregular particles dispersed over the Cu-rich matrix consist of iron-rich particles that come from the baseplate at the weld interface. No signs of new intermetallic phases are identified over these regions, which agree well with the limited mutual solubility of Cu and Fe [34].

Figure 6 presents the EBSD-based inverse pole figure (IPF) of a vortex zone. The material inside the vortex region and in the neighbouring areas has different microstructures, which are related to the different thermomechanical conditions experienced by the material in these regions. The SS presents a strongly deformed microstructure, meeting the microstructure often observed in interfacial waves [35–37]. However, equiaxed grains are observed in a copper strip in the vicinity of the vortex region, suggesting recrystallisation

**Table 4** Results of the EDS analysis (at.%) conducted in the matrix of the vortex regions

| Weld | Figure | Regions | Cu | Fe | Cr | Ni |
|---|---|---|---|---|---|---|
| LD | Figure 4c | 1 | 70.22 | 21.53 | 6.31 | 1.94 |
| | | 2 | 70.21 | 21.55 | 6.12 | 2.12 |
| HD | Figure 4d | 3 | 72.25 | 20.32 | 5.27 | 2.17 |
| | | 4 | 72.77 | 19.72 | 4.87 | 2.64 |

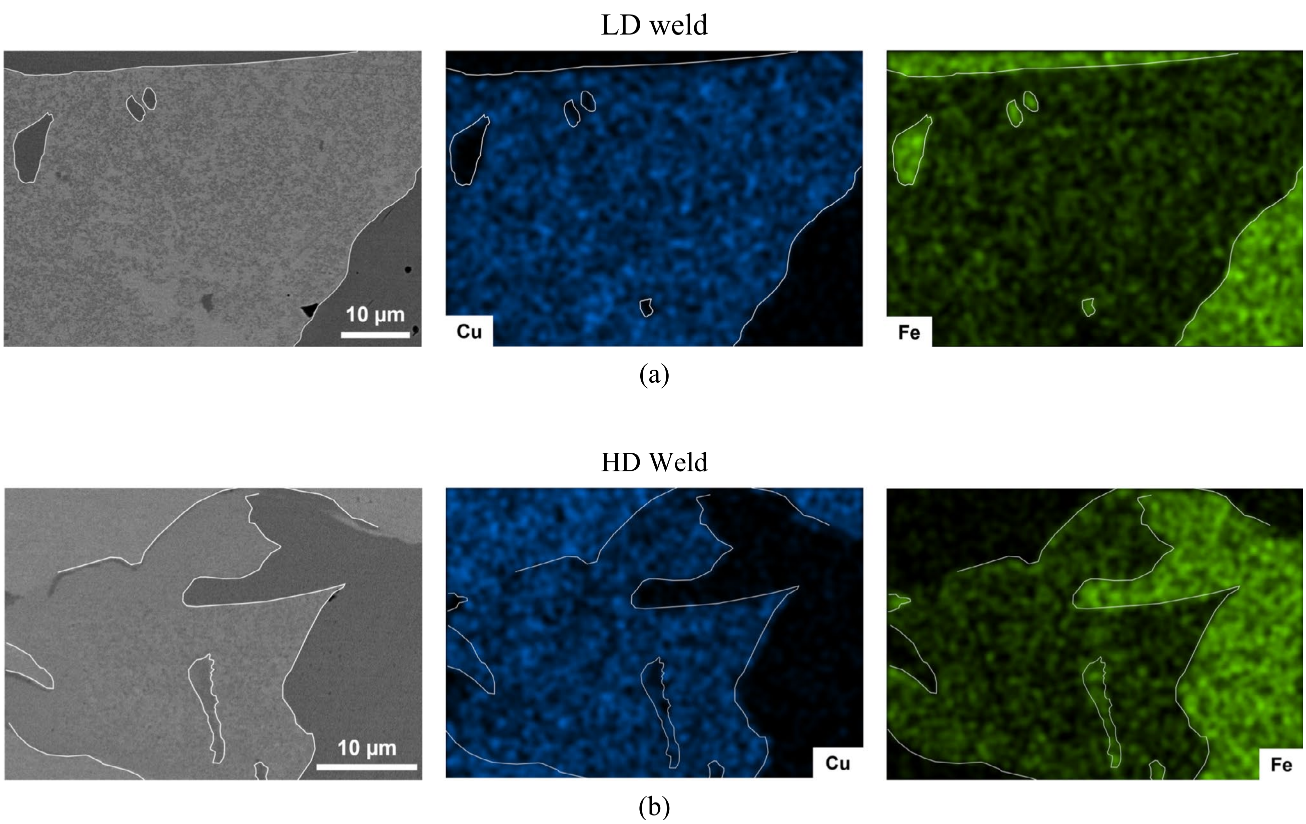


**Fig. 5** EDS elemental mapping of the vortex zones: **a** LD series, **b** HD series

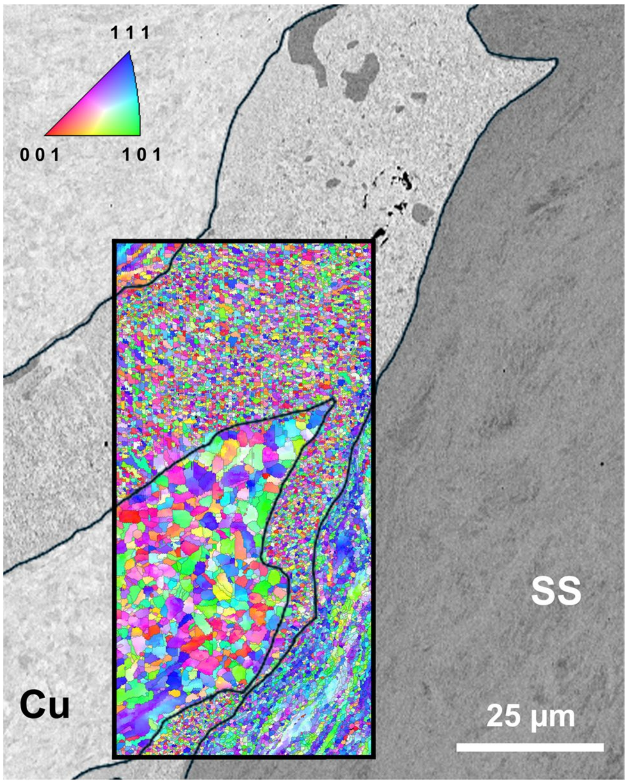


Fig. 6 EBSD-based IPF of a vortex region of the LD weld series

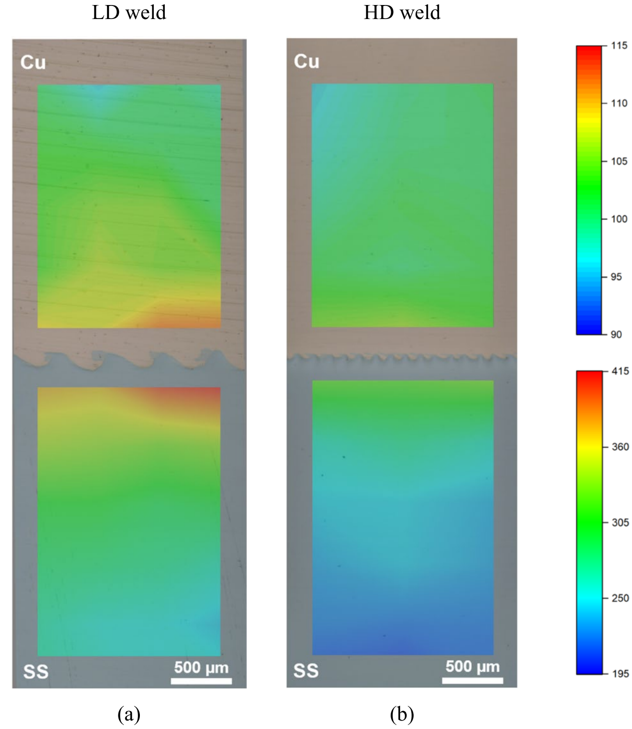


Fig. 7 Hardness ($HV_{0.2}$) maps along the longitudinal cross-section of the welds: **a** LD weld, **b** HD weld

despite the instantaneous nature of EXW. As this strip is very close to the vortex zone, an extremely high plastic strain occurs in this region, driving the recrystallisation of the material. In good agreement with this, a strongly refined microstructure is discernible in the vortex region, meeting the temperature and plastic strain peaks. The extreme plastic strain facilitated the nucleation in the vortex zone, which promoted a decrease in the size of the newly generated grains. The refinement of the microstructure was further driven by the very high heat and cooling rates experienced by the material at the weld interface. Microstructure refinement at the weld interface was reported for EXW of different material combinations, such as aluminium-steel [27], titanium-steel [32], and niobium-steel [38].

### 3.3 Weld mechanical properties

The hardness maps ($HV_{0.2}$) obtained along the longitudinal cross-section of the welds are illustrated in Fig. 7a and b. Considering the original hardness of the welded alloys (Cu, 94 $HV_{0.2}$; SS, 188 $HV_{0.2}$), the figure shows that the hardening effect is much more extensive in the SS than in Cu. While almost the entire SS plate experienced an increase in hardness, hardening was noticed only closer to the weld interface for the Cu plate. Even in this region, the hardening effect on both materials was different, with the SS presenting a much stronger hardening rate, reaching about twice the original hardness of this material. This result is consistent with the microstructure of the SS at the weld interface, composed of fine and elongated plastically deformed grains. Austenitic stainless steels are known for their capacity for work hardening through deformation, which can lead to considerably higher hardness values.

Table 5 displays the results of localised hardness measurements performed at the weld interface (in the regions indicated in Fig. 3). It shows that significantly higher hardness values were registered for the LD series, both for the Cu and SS. In fact, comparing the hardness of both series, an important influence of the welding conditions on material

Table 5 Localised interfacial hardness and maximum tensile-shear load of the welds

| Weld series | Hardness ($HV_{0.05}$) | Maximum load (kN) |
|---|---|---|
| LD | $H_1$, 104 (Cu) | 12.7–13.6 |
| | $H_2$, 125 (Cu) | 13.1[a] |
| | $H_3$, 206 (Cu/SS) | |
| | $H_4$, 538 (SS) | |
| HD | $H_5$, 106 (Cu) | 11.3–12.0 |
| | $H_6$, 285 (SS) | 11.5[a] |
| | $H_7$,104 (Cu) | |

[a]Average maximum load computed among the tested specimens

hardening is noted. The more intense and more extensive hardening observed for the LD weld series is associated with the higher $V_p$ and, consequently, the higher ΔKE registered for this series. The strongest collision promoted a more intense plastic strain at the weld interface, leading to a stronger hardening effect in the materials.

Table 5 shows the maximum load values (maximum load range and average maximum load) registered for both weld series in tensile-shear testing. The LD weld series presented a higher maximum load than the HD series. However, despite the differences in the maximum load, both weld series present similar failure characteristics. As illustrated in Fig. 8, which shows DIC distribution maps of a specimen from the HD series, the failure of the welds took place in the copper region outside the weld zone, indicating that the weld zone is stronger than the lower-strength parent material. This shows that excellent interfacial bonding was achieved for both the LD and HD weld series.

The differences in strength displayed by the weld series are associated with the different hardening rates induced by the impact, which agree well with the hardness results. The higher $V_p$ and ΔKE values registered for the LD series

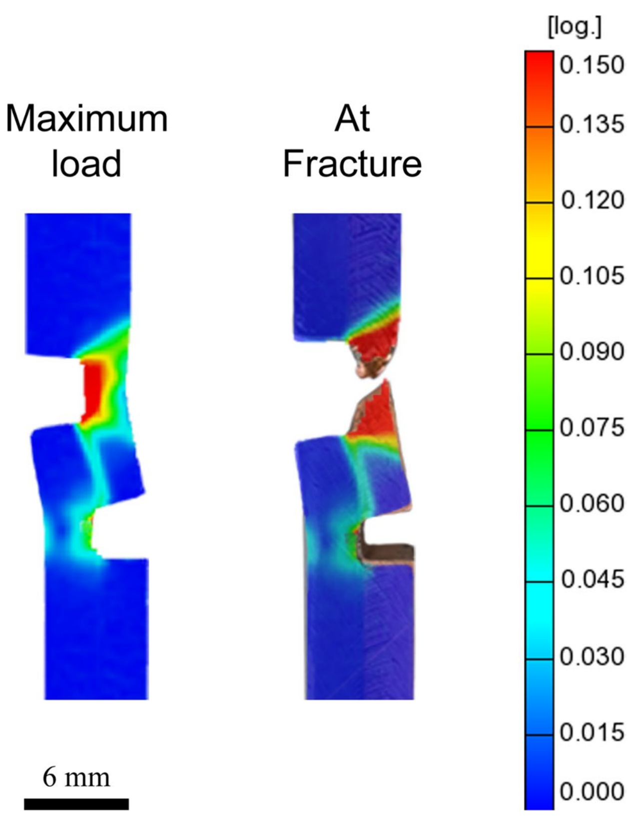


**Fig. 8** Tensile-shear behaviour of the welds—DIC strain distribution map of a specimen from the HD weld series at the maximum load and at fracture

promoted a more substantial plastic deformation, which resulted in a harder and more resistant copper region. For the tested specimen geometry, the LD explosive mixture yielded better welding conditions, resulting in welds with higher strength. It is also important to stress that very good welding conditions were achieved using these explosive mixtures, enabling the production of high-quality welds between two materials with significantly different physical properties without the need for expensive interlayer plate materials that would increase the cost and weight of the welded joint. Furthermore, the results indicate that the energetic material is crucial not only for achieving good weld joint quality, but also that it can be optimised to enhance the overall strength of the component through a general increase in hardness.

## 4 Conclusions

This work aimed at studying the influence of the energetic mixture on the quality of copper/stainless steel clads produced by EXW. The following conclusions can be drawn:

- Successful Cu-SS joining by EXW can be achieved for a detonation velocity range of 2400 and 3300 $m.s^{-1}$, without the use of expensive interlayer materials.
- Cu-SS clads presented a smoother surface finish when produced using energetic mixtures based on ammonium nitrate aqueous solution sensitised with expanded polystyrene spheres, rather than when produced with ANFO.
- The morphological pattern of the Cu-SS interfacial waves is strongly determined by disparities in the physical properties of the welded materials and their relative position in the joint. The wave geometrical parameters mainly depend on the impact parameters.
- Because of the extreme plastic strain and peak temperature achieved in the material vortex zones, these regions are composed of a Cu-rich matrix with iron-rich particles scattered over it and present a quite refined equiaxed microstructure.
- Interfacial hardening of the welds is strongly affected by the explosive mixture. Hence, the energetic material can be optimised to enhance the overall strength of the component.

**Author contribution** I. Galvão: conceptualisation; methodology; data curation; formal analysis; investigation; writing original draft; and writing, review and editing. G. H. S. F. L. Carvalho: conceptualisation; methodology; visualisation; investigation; writing, original draft; and writing, review and editing. R. M. Leal: conceptualisation, methodology, investigation, and writing—review and editing. R. Mendes: resources; investigation; writing, review and editing; and funding acquisition. All authors read and approved the final manuscript.

**Funding** Open access funding provided by Università degli Studi di Firenze within the CRUI-CARE Agreement. This research is sponsored by national funds through FCT—Fundação para a Ciência e a Tecnologia, under projects UID/00285—Centre for Mechanical Engineering, Materials and Processes, LA/P/0112/2020. This research was also funded by Fundação para a Ciência e a Tecnologia, I.P. (FCT,https://ror.org/00snfqn5816) under grant UIDB/50022/2020__https://doi.org/10.54499/UIDB/50022/2020; UIDP/50022/2020https://doi.org/10.54499/UIDP/50022/2020and LA/P/0079/2020https://doi.org/10.54499/LA/P/0079/2020.

**Data availability** Data will be made available upon request.

## Declarations

**Conflict of interest** The authors declare no competing interests.



## References

1. Wang Y, Li X, Wang X, Yan H (2018) Fabrication of a thick copper-stainless steel clad plate for nuclear fusion equipment by explosive welding. Fusion Eng Des 137:91–96. https://doi.org/10.1016/j.fusengdes.2018.08.017
2. Loureiro A, Carvalho GHSFL, Galvão I, et al (2021) Chapter 6 - Explosive welding. In: da Silva L, El-Zein M, Martins PBT-AJP (eds) Advanced joining processes: welding, plastic deformation, and adhesion. Elsevier, pp 207–237
3. Durgutlu A, Gülenç B, Findik F (2005) Examination of copper/stainless steel joints formed by explosive welding. Mater Des 26:497–507. https://doi.org/10.1016/j.matdes.2004.07.021
4. Durgutlu A, Okuyucu H, Gulenc B (2008) Investigation of effect of the stand-off distance on interface characteristics of explosively welded copper and stainless steel. Mater Des 29:1480–1484. https://doi.org/10.1016/j.matdes.2007.07.012
5. Bina MH, Dehghani F, Salimi M (2013) Effect of heat treatment on bonding interface in explosive welded copper/stainless steel. Mater Des 45:504–509. https://doi.org/10.1016/j.matdes.2012.09.037
6. Liu Y, Li C, Hu X et al (2019) Explosive welding of copper to high nitrogen austenitic stainless steel. Metals 9:339. https://doi.org/10.3390/met9030339
7. Zhu L, Zhou Q, Song C et al (2024) Microstructure and mechanical properties of T2 copper /316L stainless steel explosive welding composite with small size wavy interface. J Mater Res Technol 28:668–682. https://doi.org/10.1016/j.jmrt.2023.12.031
8. Feng R, Zhao W, Gan K et al (2022) Investigation of interface microstructure and properties of copper/304 stainless steel fabricated by explosive welding. J Mater Res Technol 18:2343–2353. https://doi.org/10.1016/j.jmrt.2022.03.142
9. Carvalho GHSFL, Galvão I, Mendes R (2023) The role of physical properties in explosive welding of copper to stainless steel. Def Technol 22:88–98. https://doi.org/10.1016/j.dt.2022.08.016
10. Song X, Yang Y, Cheng Y et al (2024) Study on copper-stainless steel explosive welding for nuclear fusion by generalized interpolated material point method and experiments. Eng Anal Boundary Elem 160:160–172. https://doi.org/10.1016/j.enganabound.2024.01.003
11. Mendes R, Ribeiro J, Plaksin I et al (2014) Differences between the detonation behavior of emulsion explosives sensitized with glass or with polymeric micro-balloons. J Phys Conf Ser 500:052030. https://doi.org/10.1088/1742-6596/500/5/052030
12. Pimenta J, Quaresma J, Ribeiro J, Mendes R (2023) Detonation characterization of low-density emulsion explosives. Propellants Explos Pyrotech. https://doi.org/10.1002/prep.202300046
13. Mendes R, Ribeiro JB, Loureiro A (2013) Effect of explosive characteristics on the explosive welding of stainless steel to carbon steel in cylindrical configuration. Mater Des 51:182–192. https://doi.org/10.1016/j.matdes.2013.03.069
14. Quaresma J, Deimling L, Campos J, Mendes R (2020) Active and passive optical fiber metrology for detonation velocity measurements. Propellants Explos Pyrotech 45:921–931. https://doi.org/10.1002/prep.201900197
15. Carvalho GHSFL, Galvão I, Mendes R et al (2020) Aluminum-to-steel cladding by explosive welding. Metals (Basel) 10:1–18. https://doi.org/10.3390/met10081062
16. Carvalho GHSFL, Galvão I, Mendes R et al (2020) Explosive welding of aluminium to stainless steel using carbon steel and niobium interlayers. J Mater Process Technol 283:116707. https://doi.org/10.1016/j.jmatprotec.2020.116707
17. Broughton W (2012) Testing the mechanical, thermal and chemical properties of adhesives for marine environments. Adhesives in marine engineering 99–154. https://doi.org/10.1533/9780857096159.2.99
18. Leitão C, Galvão I, Leal RM, Rodrigues DM (2012) Determination of local constitutive properties of aluminium friction stir welds using digital image correlation. Mater Des. https://doi.org/10.1016/j.matdes.2011.07.009
19. Kennedy JE (1970) Gurney energy of explosives: estimation of the velocity and impulse imparted to driven metal. Albuquerque and Livermore
20. El-Sobky (1983) Mechanics of explosive welding. In: Blazynski TZ (ed) (ed) Explosive Welding, Forming and Compaction. Applied Science Publishers, pp 189–217
21. Patterson RA (1993) Fundamentals of explosion welding. ASM Handbook—Volume 6: Welding, Brazing and Soldering. ASM International, Materials Park, pp 160–164
22. Cooper PW (1996) Explosive engineering. Wiley-VCH, New York
23. Mendes R, Plaksin I, Ribeiro JB, et al (2016) Effect of detonation characteristics on the properties of the explosive welding interface. In: EPNM-2016-XIII International symposium on explosive production of new materials: science, technology, business and innovations. Coimbra, p 109
24. Zakharenko ID (1972) Critical conditions in detonation welding. Combust Explos Shock Waves 8:341–345. https://doi.org/10.1007/BF00742312
25. Efremov VV, Zakharenko ID (1976) Determination of the upper limit to explosive welding. Combust Explos Shock Waves 12:226–230. https://doi.org/10.1007/BF00744893
26. Athar MMH, Tolaminejad B (2015) Weldability window and the effect of interface morphology on the properties of Al/Cu/Al laminated composites fabricated by explosive welding. Mater Des 86:516–525. https://doi.org/10.1016/j.matdes.2015.07.114
27. Chu Q, Xia T, Zhao P (2022) Interfacial investigation of explosion-welded Al/steel plate: the microstructure, mechanical properties and

residual stresses. Materials Science and Engineering: A 833:142525. https://doi.org/10.1016/j.msea.2021.142525
28. Bataev IA, Lazurenko DV, Tanaka S et al (2017) High cooling rates and metastable phases at the interfaces of explosively welded materials. Acta Mater 135:277–289. https://doi.org/10.1016/j.actamat.2017.06.038
29. Carvalho GHSFL, Mendes R, Leal RM (2017) Effect of the flyer material on the interface phenomena in aluminium and copper explosive welds. Mater Des 122:172–183. https://doi.org/10.1016/j.matdes.2017.02.087
30. Bataev IA, Bataev AA, Mali VI et al (2014) Structural changes of surface layers of steel plates in the process of explosive welding. Met Sci Heat Treat 55:509–513. https://doi.org/10.1007/s11041-014-9663-7
31. Yang M, Xu J, Ma H et al (2021) Microstructure development during explosive welding of metal foil: morphologies, mechanical behaviors and mechanisms. Compos Part B Eng 212:108685. https://doi.org/10.1016/j.compositesb.2021.108685
32. Zhou Q, Liu R, Chen P, Zhu L (2021) Microstructure characterization and tensile shear failure mechanism of the bonding interface of explosively welded titanium-steel composite. Mater Sci Eng A 820:141559. https://doi.org/10.1016/J.MSEA.2021.141559
33. Galvão I, Carvalho GHSFL, Pimenta J et al (2024) Structural analysis of aluminium-titanium-stainless steel three-layer composites produced by explosive welding. Weld World 68:2911–2925. https://doi.org/10.1007/s40194-024-01830-5
34. Zhang C, Chen C, Huang L et al (2021) Microstructure and properties of Cu-Fe alloys fabricated via powder metallurgy and rolling. Powder Metall 64:308–320. https://doi.org/10.1080/00325899.2021.1890403
35. Carvalho GHSFL, Galvão I, Mendes R et al (2018) Influence of base material properties on copper and aluminium–copper explosive welds. Sci Technol Weld Join. https://doi.org/10.1080/13621718.2017.1417783
36. Carvalho GHSFL, Galvão I, Mendes R et al (2019) Microstructure and mechanical behaviour of aluminium-carbon steel and aluminium-stainless steel clads produced with an aluminium interlayer. Mater Charact. https://doi.org/10.1016/j.matchar.2019.109819
37. Paul H, Chulist R, Miszczyk M et al (2020) Towards a better understanding of the phase transformations in explosively welded copper to titanium sheets. Mater Sci Eng A. https://doi.org/10.1016/j.msea.2020.139285
38. Xu J, Ma H, Yang M et al (2022) Experimental and numerical investigations on the microstructural features and mechanical properties of explosive welded niobium-steel interface. Mater Des 218:110716. https://doi.org/10.1016/j.matdes.2022.110716